Research Article | Vol. 29, No. 2 / 18 January 2021 / Optics Express 2769
Optics EXPRESS

Time-resolved HO_2 detection with Faraday rotation spectroscopy in a photolysis reactor

CHU C. TENG,[1] CHAO YAN,[2,4] ARIC ROUSSO,[2,4] HONGTAO ZHONG,[2,4] TIMOTHY CHEN,[2] ERIC J. ZHANG,[1,3] YIGUANG JU,[2] AND GERARD WYSOCKI[1,*]

[1]*Department of Electrical Engineering, Princeton University, Princeton, NJ 08540, USA*
[2]*Department of Mechanical and Aerospace Engineering, Princeton University, Princeton, NJ 08540, USA*
[3]*Currently at IBM Thomas J. Watson Research Center, 1101 Kitchawan Rd, Yorktown Heights, NJ 08540, USA*
[4]*These authors contributed equally to this work*
[*]*gwysocki@princeton.edu*

Abstract: Faraday rotation spectroscopy (FRS) employs the Faraday effect to detect Zeeman splitting in the presence of a magnetic field. In this article, we present system design and implementation of radical sensing in a photolysis reactor using FRS. High sensitivity (100 ppb) and time resolved *in situ* HO_2 detection is enabled with a digitally balanced acquisition scheme. Specific advantages of employing FRS for sensing in such dynamic environments are examined and rigorously compared to the more established conventional laser absorption spectroscopy (LAS). Experimental results show that FRS enables HO_2 detection when LAS is deficient, and FRS compares favorably in terms of precision when LAS is applicable. The immunity of FRS to spectral interferences such as absorption of hydrocarbons and other diamagnetic species absorption and optical fringing are highlighted in comparison to LAS.

1. Introduction

Sensitive and reliable detection of key intermediate species is critical for improving and validating our understanding and modeling of combustion and plasma chemistry [1–3]. In particular, the drive towards next-generation engines with reduced emissions and increased efficiency has led to interests in low-temperature and high pressure chemical kinetics [3–6]. A direct motivation for the construction of our photolysis system is to study the reactions between fuels and the electronically excited singlet oxygen atom, $O(^1D)$, whose significance has been elaborated in prior literatures [3,5–11]. The challenge of detecting trace radical species in a complicated environment such as a combustion or plasma reactor is the inevitable presence of many species simultaneously. For kinetic studies, selective detection of the target species as the chemistry evolves (often within milliseconds) is important, therefore demanding measurement techniques that can provide both high sensitivity and high selectivity.

Fortunately, due to the unpaired electron in free radicals, their paramagnetic property can be exploited to distinguish them from diamagnetic species. Some of the first applications of this technique were introduced in biological systems where uncontaminated measurements are not possible [12]. More recently, FRS has been adopted for the detection of oxygen and NO [13–17] as well as for other radicals [18,19]. Steady state HO_2 measurements using FRS were previously demonstrated near the exit of a laminar flow reactor at atmospheric pressure [20–22]. Prior works focused on sensitivity enhancement of HO_2 detection through magnetic field modulation and phase-sensitive lock-in detection using FRS. This approach is however not suitable for transient systems due to the low achievable magnetic field modulation frequency (below 1 kHz) given the size of the electromagnetic coils, which limits the detection time resolution to the milliseconds timescale. In this paper, we eliminated the need for magnetic field modulation while providing

#413063 https://doi.org/10.1364/OE.413063
Journal © 2021 Received 23 Oct 2020; revised 23 Dec 2020; accepted 23 Dec 2020; published 15 Jan 2021

Optics EXPRESS

immunity to spectral interference by developing a digitally balanced FRS detection scheme. In this case temporal resolution is only limited by the laser wavelength scanning (or wavelength modulation) rate and by the data acquisition rate. We evaluate the advantages of the balanced FRS scheme for HO_2 detection in a photolysis reactor. Characteristic concerns in such applications include laser intensity instabilities and drifting background spectral structures are explored and the suitability of FRS to address them is confirmed against conventional laser absorption spectroscopy (LAS) that is commonly used for monitoring of fast transient chemical processes.

2. Experimental setup

The setup shown in Fig. 1 can be categorized into 3 key parts: the ultra-violet (UV) photolysis setup that initiates the chemical reactions, the FRS setup that performs HO_2 detection along with the quasi real-time digitally balanced detection algorithm, and the QCL frequency stabilization setup for line-locked operation. It should be mentioned that the system can also perform conventional LAS without alteration, and this capability is leveraged to support our evaluation of the FRS detection in comparison to conventional LAS under the same experimental conditions. The core of the UV photolysis setup is a quartz photolysis flow cell, in which a UV photolysis laser (ND:YAG laser operating at 266 nm) is used to generate the excited oxygen singlet $O(^1D)$ from O_3. Note that the UV laser beam is expanded to improve uniformity of intensity distribution as well as increase the volume in which reactions occur. The $O(^1D)$ reacts with fuels of interest, forming radicals such as HO_2 and OH on microsecond to millisecond timescales.

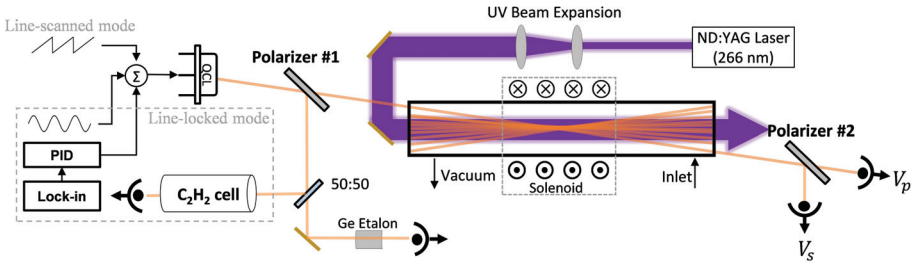

Fig. 1. System setup. The photolysis reactor is equipped with a 21-pass Herriot cell for the mid-IR probe beam while allowing the ultra-violet photolysis beam directly through the center of the cell. A solenoid around the center region of the cell generates an axial magnetic field for FRS measurement. Polarizer #1 ensures linearly polarized light incident on the cell while Polarizer #2 is used to split the exiting beam into orthogonal polarizations, each of which is detected by a photodetector. In the laser scan mode, a germanium etalon is used to calibrate optical frequency scan. Optionally, a reference cell filled with C2H2 can be used for frequency reference for line-locked operation.

Two custom-designed UV-grade CaF_2 windows cap the ends of the cylindrical cell. The windows have a diameter of 66 mm, with a 40 mm diameter clearance at the center for the photolysis laser to pass directly through the reactor. The inner surfaces of the windows are concave with a radius of curvature of 50 cm and a 1.3 cm wide band of protected gold coats the perimeter to form a Herriot multi-pass cell (MPC). The single mode quantum cascade laser (QCL) for HO_2 detection enters the reactor through a slit in the gold coating, followed by 21 passes within the reactor. Since we are probing the reactions that occur within the UV beam profile (ensuring that diffusion is negligible on the timescale of interest), the IR beam path intercepted by the UV beam profile defines the effective optical pathlength over which the radicals are formed and can be detected by LAS.

To induce Faraday rotation, a solenoid is incorporated around the photolysis reactor to generate an axial magnetic field. In this setup, the length of the solenoid has been designed to cover the

Optics EXPRESS

overlapping region between the UV profile and the IR beam as illustrated in the setup schematic. Calculations show that comparable detection pathlengths have been achieved for both FRS (6.3 m) and LAS (6.4 m) as explained in the Supplement 1. Note that for accurate modeling of the FRS signal, the magnetic field profile is measured along the center axis of the reactor so that nonuniformities of the magnetic field distribution can also be accounted for in the modeling of the HO_2 FRS spectrum (also explained in the Supplement 1).

3. Faraday rotation spectroscopy

The FRS detection mechanism is based on the Faraday Effect: when linearly polarized laser light resonantly interacts with paramagnetic molecules in a coaxial external magnetic field, magnetically induced circular birefringence (MCB) causes rotation of the polarization plane of the transmitted light, which is proportional to the concentration of the target species. This polarization rotation is detected by first ensuring the incident light is linearly polarized (with Polarizer #1), then using another polarizer (Polarizer #2, or an analyzer) to convert polarization rotation into optical intensity change. Here Polarizer #2 is set to 45 with respect to the axis of Polarizer #1, allowing equal splitting of the p and s polarizations in the absence of Faraday rotation signal, which are captured simultaneously by two optical detectors.

Following the derivation using Jones matrix as described in past literatures [14,23], the signals measured by the two detectors can be written as:

$$V_s = \frac{R_s P_0 \beta^2}{2}(\cosh 2\kappa + \cos 2\Theta \cos 2\theta + \sin 2\Theta \sin 2\theta); \tag{1}$$

$$V_p = \frac{R_p P_0 \beta^2}{2}(\cosh 2\kappa - \cos 2\Theta \cos 2\theta - \sin 2\Theta \sin 2\theta). \tag{2}$$

In our setup, the transmitted channel corresponds to the p polarization while the reflected channel corresponds to s polarization. The photodetectors' conversion between incident optical power and voltage output is captured in R_s and R_p, with s and p signifying the corresponding polarization of the detection channel. P_0 is the incident optical power; β represents the attenuation of light due to sample absorption; κ represents the effect of molecular circular dichroism (MCD), which is the difference in absorption between the left and right handed circular polarization induced by the applied external magnetic field; Θ is the polarization rotation due to molecular circular birefringence (MCB), which is the Faraday rotation signal we intent to measure; θ is the angle between the axis of Polarizer #1 and Polarizer #2. Note that we have omitted influence of polarizer imperfections as the polarizers used in this setup have high extinction ratios (WP25MIRC, Thorlabs, Inc.). Moreover, since the analyzer is set to 45 there is a large amount of light in both polarization states, which makes the polarizer extinction of lesser importance. By observing the signs of the terms in Eq. (1) and (2), the differential nature of this technique becomes clear: while the MCD is common mode, the contribution of MCB is opposite for the two detection channels. Taking the difference between the two detector signals, we obtain

$$V_{\text{diff}} = \frac{P_0 \beta^2}{2}[(R_s - R_p)\cosh 2\kappa + (R_s + R_p)(\cos 2\Theta \cos 2\theta + \sin 2\Theta \sin 2\theta)]. \tag{3}$$

If the two detectors have identical responsivity and gain, i.e. $R_s = R_p = R$, then the effect of MCD is canceled when taking the difference between the two channels:

$$V_{\text{diff}} = P_0 \beta^2 R(\cos 2\Theta \cos 2\theta + \sin 2\Theta \sin 2\theta). \tag{4}$$

This can be achieved by employing auto balancing detectors that have high common mode suppression ratio (CMRR). Since availability of proper balanced detectors in the mid-IR is

Optics EXPRESS

quite limited and costly, we have developed a digital balancing scheme that is performed in the post-processing such that R_p is scaled by a factor r that leads to $R_s \approx rR_p = R$. This procedure can be fast and effectively performed following data sampling and sufficient CMRR is routinely achieved. In general, the scaling factor r has an optical frequency dependence that needs to be accounted for to balance the spectra obtained by two separate detectors. In our experiments $r(\nu)$ is determined from the spectral ratio between the two detection channels during background acquisition (detailed procedure used for digital balancing is explained in the Supplement 1).

Now, setting the polarizer angle to $\theta = 45°$ further simplifies Eq. (4) to

$$V_{\text{diff},45°} = P_0\beta^2 R \sin 2\Theta. \tag{5}$$

Under the same balanced 45° detection condition, the average of the two detectors' signals is

$$V_{\text{avg},45°} = \frac{P_0\beta^2 R \cosh 2\kappa}{2}. \tag{6}$$

The absorption background along with parameters related to the detectors can be removed through power normalization:

$$V_{\text{norm},45°} = \frac{V_{\text{diff},45°}}{V_{\text{avg},45°}} = \frac{2\sin 2\Theta}{\cosh 2\kappa}. \tag{7}$$

For $\kappa << 1$, which is a valid assumption for small sample absorption, $\cosh 2\kappa \approx 1$ and the term due to MCD becomes negligible. The Faraday rotation signal can therefore be obtained from $\Theta \approx V_{\text{norm},45°}/4$ for small rotation angle assuming proper signal balancing.

In the current configuration one can simply disable the magnetic field so that Eq. (1) and (2) reduce to the same form, indicating that either channel would equally yield the absorption signal. In the presence of the magnetic field, the absorption signal can also be approximated using $V_{\text{avg},45°}$, where the influence of MCB is eliminated. This feature allows simultaneous acquisition of the absorption spectrum and the Faraday rotation spectrum, which enables direct comparison between LAS with FRS under identical experimental conditions.

4. Signal acquisition

We acquire 5 ms of background data before the UV photolysis pulse and 15 ms of kinetic data following the photolysis. The photolysis events are repeated every 4 s to ensure that the system has re-normalized. Typically, 50 to 100 such photolysis events are acquired consecutively and averaged to improve detection precision. A MATLAB script has been developed to interface with a fast digitizer (GaGe FCiX Razor) such that acquisition is properly triggered with respect to the photolysis laser, and the down time between two consecutive photolysis events are utilized to perform HO_2 concentration retrieval for quasi real-time diagnosis. For each measurement, the algorithm calculates $V_{\text{norm},45°}$ with the balancing ratio $r(\nu)$ obtained from the averaged background data (see the Supplement 1). In the wavelength-scanned mode of the instrument operation, the single mode QCL is driven by a sawtooth waveform to produce the FRS spectrum. A one-inch germanium etalon is used to linearize the frequency axis, and HO_2 concentration is retrieved through FRS spectral fit.

As we show later in this paper, the immunity of FRS to spectral interference permits FRS to be operated also in a line-locked mode. In this mode, the QCL is modulated so that its optical frequency can be locked to the peak of an HO_2 transition by performing wavelength modulation spectroscopy (WMS) on acetylene (C_2H_2) transitions. The pre-photolysis measurement is used as the background and averaged to perform balancing of the photodetector signals at a fixed spectral position, followed by digital demodulation and subtraction of the two detection channels to obtain the HO_2 second harmonic FRS signal. This operation mode can potentially enable improved time resolution that is primarily limited by the modulation frequency and can be extended to GHz if direct QCL current modulation is implemented.

Optics EXPRESS

5. Comparison between FRS and LAS

In rapid sensing experiments such as in a photolysis reactor or a shock-tube [24–27], slowly drifting baselines can in some cases be subtracted. However, signals due to molecules other than the target species and other noise sources that occur on short time scales directly affect accuracy and precision of the measurements.

There are a few scenarios regarding spectral interference in spectroscopic measurements. In the most optimistic scenario, the interfering species occur as a static background that can be pre-recorded and subtracted during subsequent measurements. This is however an invalid assumption when the interfering species are formed or dissipated during the chemical reactions under study.

In the second scenario, the evolution of the interference species is on a similar timescale as that of the target species, but their spectra can be accurately modeled and therefore accounted for through nonlinear regression. In this case, conventional LAS is applicable and can serve as the benchmark to establish the validity of FRS measurements. Note that since spectral fitting is used to estimate the interference, line-locked WMS measurements would be difficult to apply in such a scenario.

In the third scenario the spectral interference is assumed to be changing and proper modeling cannot be performed. For example, larger hydrocarbon fuels are of great interest in the combustion and plasma chemistry community, but line-by-line parameters are generally unavailable and thus their interference cannot be easily accounted for. In addition, the general practice of selecting spectral regions free of interference becomes challenging due to their broadband spectral signatures. In such a scenario a measurement that provides additional selectivity is preferred and in this work, FRS is used to clearly differentiate paramagnetic radicals from diamagnetic interference species. In the following sections we first validate FRS using LAS in the second scenario, then provide an experimental demonstration of the third scenario, where FRS shows clear advantage over LAS.

Using the setup shown in Fig. 1, LAS and FRS can be implemented simultaneously assuring a fair comparison. For experimental demonstration of the second spectral interference scenario, the reaction between $O(^1D)$ and C_2H_2 is chosen because C_2H_2 transitions are well-documented in our spectral region and can be distinguished from the LAS spectrum of HO_2 through spectral post-processing. In the following experiment the reactor pressure was maintained at 150 Torr.

Each spectrum is obtained by sawtooth scanning of the QCL from 1396.86 cm^{-1} to 1396.96 cm^{-1} at a rate of 10 kHz. In Fig. 2(a), the LAS transmission spectra over the 20 ms acquisition averaged from 100 consecutive photolysis events are presented as a vertical cascade to illustrate the fast dynamics of the spectral signal. Note that the averaged spectral background from the pre-photolysis acquisition (from −5 ms to 0 ms detection time) is used as a background that is subtracted throughout the spectral cascade. Periodic baseline intensity fluctuations appearing as "ripples" along the time axis are observed with a period of 0.5 ms to 1 ms, and we suspect that is due to parasitic etalons in the system. If this dataset with simple pre-photolysis background subtraction is used to extract the time evolution of HO_2 concentration during a photolysis event, the ripples are clearly transferred onto the extracted HO_2 concentrations shown by the gray trace in Fig. 3(a). Additionally there is a clear baseline shift that results in a retrieved concentration bias. Therefore, it has been determined that at least a first order baseline correction must be included into the fitting model to suppress these unwanted effects.

An example spectrum that contains strong HO_2 signal (acquired 0.8 ms after the photolysis pulse) is chosen for demonstration of spectral analysis based on the first order baseline along with contributions from both C_2H_2 and HO_2 absorption. The fitting results are shown in Fig. 2(c). The component C_2H_2 and HO_2 transmission profiles are plotted in the top panel along with the overall fit to the measured data; the fit residual is shown in the bottom panel. It is evident that properly accounting for spectral interferences from C_2H_2 as well as for the baseline drift results

Optics EXPRESS

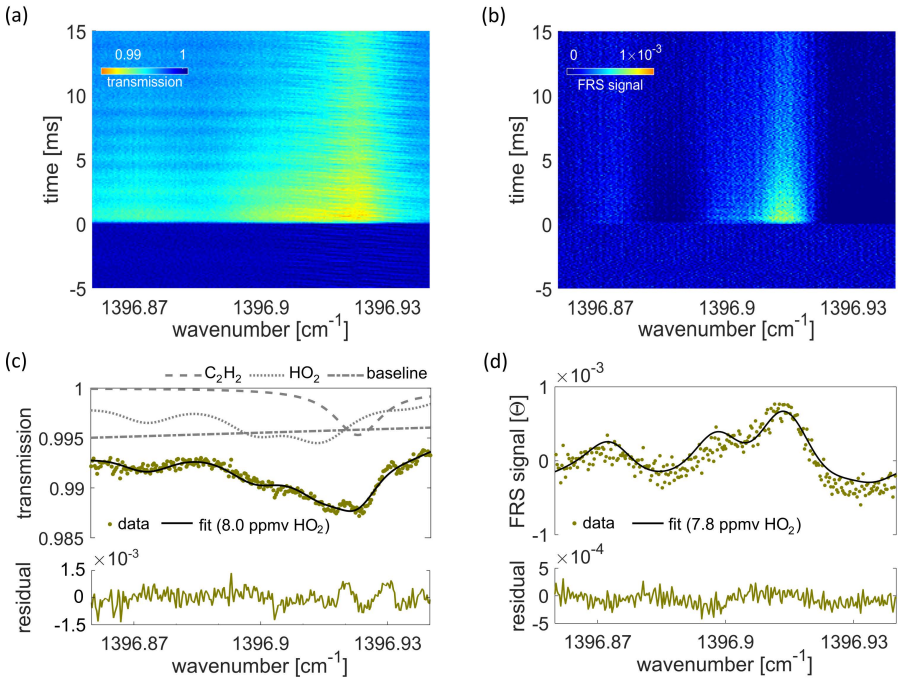

Fig. 2. Comparison of HO_2 absorption measurement and Faraday rotation measurement. Experimental conditions: 150 Torr with C_2H_2 as the fuel. (a) Vertical cascade of the background normalized transmission spectra for a full photolysis acquisition of 20 ms containing both the HO_2 absorption and residual C_2H_2 absorption. (b) Vertical cascade of the FRS spectra; only HO_2 signals are observed. (c) Least-squares fit of a spectrum from (a). Top panel shows the fitted spectral contributions from HO_2, C_2H_2, and a first order baseline. The overall fitted result is plotted on top of the background removed absorption data. The bottom panel is the fit residual. (d) Top panel shows the spectral fit to the FRS HO_2 signal using the HO_2 spectrum only, and the residuals are shown in the lower panel.

in suppression of the intensity fluctuations and the concentration bias observed earlier. This is confirmed when the same data set is analyzed using FRS detection, which results in very similar HO_2 concentration time profiles as shown by the red trace in Fig. 3(a).

The FRS analysis generally provides more confident HO_2 concentration retrieval due to its high selectivity and immunity to intensity noise. This is clearly visible by comparing the spectral cascade in Fig. 2(b) measured with FRS to the LAS results in Fig. 2(a). Since FRS is a background-free differential measurement, common-mode noise such as optical fringing from the MPC, optical power fluctuations, and spectral interferences from diamagnetic species are effectively suppressed. As a result, a clean HO_2 signal (without the ripples observed in Fig. 2(a)) is observed throughout the acquisition in Fig. 2(b). Similarly, the FRS model fit in Fig. 2(d) is obtained by considering only the HO_2 FRS spectrum, while the LAS model (Fig. 2(c)) must include C_2H_2 model together with a first order baseline to suppress the intensity fluctuations and optical fringing, which results in increased complexity of the LAS model and requires more fitting parameters that can lead to unwanted crosstalk and degraded sensitivity and accuracy. A close examination of the first 5 ms of background acquisition in Fig. 3(a) reveals HO_2 concentration retrieval standard deviation of 0.3 ppmv using LAS with a first order baseline model, and 0.1 ppmv using FRS. Based on this analysis, even in the case where the spectral interference can

Optics EXPRESS

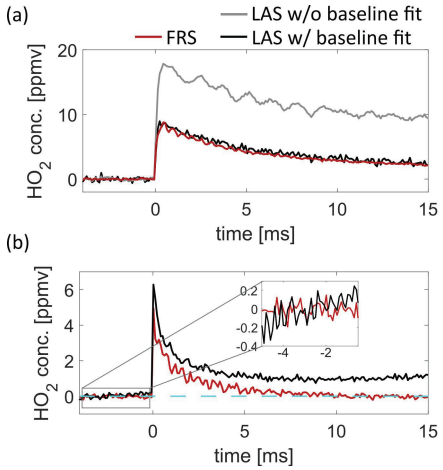

Fig. 3. Comparison between LAS and FRS. (a) HO_2 concentration retrievals from a photolysis experiment with C_2H_2 as the interfering fuel species. (b) HO_2 concentration retrievals from a photolysis experiment with propane as the interfering fuel species. In this case LAS model assumes only HO_2 absorption due to lack of accurate propane transition parameters in this spectral region. A dashed reference line (cyan) marking zero HO_2 concentration is also provided to help visualize the baseline-free detection using FRS.

be properly accounted for, FRS appears to be a more robust and advantageous method for HO_2 detection.

Now we explore the third scenario, where the spectral interference is changing during the single photolysis event and cannot be properly modeled. A sensing mechanism that can accommodate this situation is important for versatile application of the instrument. Figure 3(b) shows the HO_2 retrieval for a photolysis experiment using propane as the fuel. Unlike C_2H_2, propane cannot be accurately modeled at 150 Torr, hence the LAS fitting model contains only the HO_2 absorption profile and a polynomial baseline. Influences of a changing baseline on HO_2 retrieval is observed in the first 5 ms of LAS retrieval in Fig. 3(b), which shows slow HO_2 concentration increase even before the photolysis event. Based on prior works studying the HO_2 time profile using kinetic models [7,9], a monotonic decay in HO_2 concentration is generally expected after the immediate HO_2 generation. The leveling off and slight increase in the observed LAS retrieved HO_2 concentration clearly visible at 10–15 ms after the photolysis laser pulse in Fig. 3(b) is therefore unphysical and reflects background drifts that interfere with the extraction of HO_2 signal. Since FRS selectively detects HO_2, the influences from propane and other intermediate chemicals are suppressed. The retrieved HO_2 concentration profile maintains a consistent zero-gas background until the photolysis pulse is administered at 0 ms detection time, after which a sudden rise is followed by the expected decay in HO_2 concentration back to the initial zero baseline observed before the event.

6. Line-locked FRS

The immunity of FRS to common-mode background changes both due to spectral interference and common-mode parasitic fringes (both shown in the previous section) enables line-locked mode of operation. In principle, a line-locked detection mode allows improved time resolution since there is no need to acquire the full spectrum. This technique has also shown sensitivity advantages with the proper choice of modulation frequency to avoid noisy regions of operation [16]. Although the optimization for time resolution and sensitivity was not a focus of this work,

Optics EXPRESS

we show a proof-of-concept implementation to demonstrate the feasibility of line-locked FRS in the present system.

Conventionally, to perform laser frequency locking, the target gas is sealed in a reference cell and the molecular transition of interest is used as the frequency reference. As HO_2 is a short-lived radical that cannot be stored in a sealed cell, we resort to using a stable molecule with transitions nearby the target HO_2 transition. In this work, we use the second harmonic WMS spectrum of an C_2H_2 transition at 1396.3 cm^{-1} to perform frequency locking at the center of the HO_2 feature.

QCL modulation is performed with a 100 kHz sinusoidal waveform supplied to the analog input of the QCL driver (QCL500 OEM+, Wavelength Electronics, Inc.). The wavelength modulated light is directed through a reference cell (10 cm) containing 100% C_2H_2, and the detector signal is demodulated using a lock-in amplifier (Model 7280, Signal Recovery, Inc.). Figure 4(a) shows a simulation of the in-phase second harmonic C_2H_2 signal (dashed) along with the in-phase second harmonic HO_2 FRS spectrum (solid). The locking position is marked (in red) on the left wing of the C_2H_2 line, which coincides with the peak of the targeted HO_2 transition. It should be noted that depending on the photolysis reactor pressure, the locking position needs to accommodate varying pressure broadening and shift of the HO_2 spectrum, hence the corresponding reference cell pressure that results in the best locking condition is carefully calculated prior to experimental setup. In the simulation shown in Fig. 4(a), for example, the reference cell pressure is selected to be 100 Torr for the reactor pressure of 60 Torr.

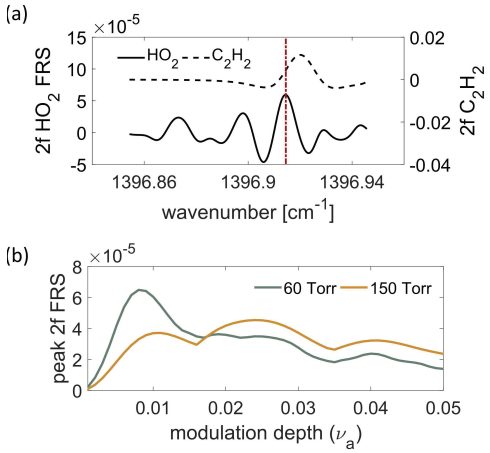

Fig. 4. (a) Simulated second harmonic absorption profile for C_2H_2 (100 Torr) and second harmonic FRS spectrum for HO_2 (60 Torr). The frequency locking position is marked in red. (b) Simulation of peak second harmonic FRS signal for 1 ppmv of HO_2 with varying modulation depth. The optimal modulation depth is determined for different cell pressures (60 Torr and 150 Torr shown here) by identifying the highest 2f FRS signal.

Furthermore, due to pressure broadening effects, the optimum modulation depth also changes according to pressure. Figure 4(b) shows the maximum in-phase FRS second harmonic signal with varying modulation depth. Due to the proximity of HO2 lines within this spectral region, Fig. 4(b) shows complex relationships between the peak second harmonic signal and the modulation depth. As the simulations indicate, the optimal modulation depth that corresponds to the maximum demodulated FRS signal is 0.008 cm−1 at 60 Torr reactor pressure while it should be increased to 0.024 cm−1 for 150 Torr reactor pressure.

With the QCL frequency stabilized to the C_2H_2 transition, we continuously acquire signals using the two detectors after the analyzer. In a photolysis experiment using methanol as the fuel, we demonstrate HO_2 concentration retrieval using line-locked FRS. Figure 5(a) shows the

Optics EXPRESS

digitally demodulated second harmonic *s* and *p* polarization signals averaged over 50 photolysis events. Common-mode signal fluctuations throughout the acquisition is clearly noticeable, which is effectively suppressed by taking the difference between the two channels as shown in Fig. 5(b). As a validity check, wavelength-scanned FRS detection is performed under the same experimental conditions and the HO_2 retrievals are plotted also in Fig. 5(b). In our case we applied 100 kHz modulation in combination with 100 µs lock-in time constant for a fair comparison between line-locked and wavelength-scanned detection results. Quantitative agreement between these two modes of FRS detection imply successful implementation of line-locked FRS. The main potential of the sinusoidally modulated line-locked operation is in its capability of achieving high time resolution as compared to sawtooth wavelength scanning. Due to modulation bandwidth restrictions of our laser current source our proof-of-concept line-locked retrieval demonstration was limited to sub-MHz modulation frequency which in combination with 100 µs lock-in time constant allowed for sub-ms time resolution. However, direct QCL current modulation can be performed up to GHz frequencies with only slight laser setup modifications, which is expected to enable time resolutions in the sub-µs regime using the same detection system.

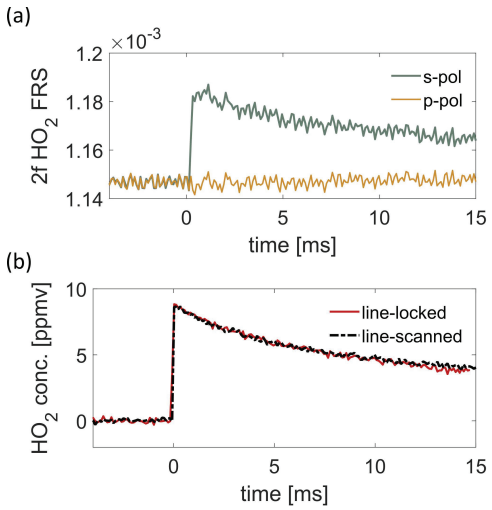

Fig. 5. (a) Demodulated second harmonic HO_2 signal of the *s*- and *p*-polarization channel during an FRS experiment with 60 Torr cell pressure and methanol as the fuel. (b) Wavelength-scanned and line-locked HO_2 retrievals under the same experimental conditions.

7. Sensitivity analysis

To improve the instrument sensitivity for measuring HO_2, especially when fine time resolution is needed, it is helpful to average over multiple photolysis events. The progression of each photolysis event is well defined by referencing to the time of the UV laser pulse, hence the HO_2 concentrations at the same detection time can be averaged over multiple events. Figure 6(a) shows 200 such events consecutively acquired while the system is operated under the same conditions. Depending on the pressure in the reactor, the amount of down time between two consecutive photolysis events varies to allow system to return to the background state. In our setup, this time interval is set to 4 s, which means an extended time elapses with increased averaging. Given the complexity of the system, it is important to perform a stability analysis to ensure that the system remains reproducible and that further averaging is meaningful.

To evaluate the effectiveness of the averaging process, Allan deviation analysis is performed on the HO_2 retrievals at each detection time. As an example, the HO_2 concentration retrieved at

Optics EXPRESS

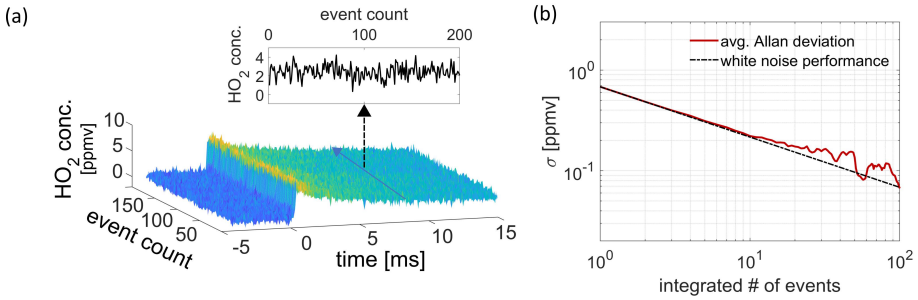

Fig. 6. (a) 200 consecutive acquisitions of HO_2 time profile. For each detection time with respect to the photolysis pulse, we examine the precision of the HO_2 concentration retrieval. For demonstration, the HO_2 retrieval at 10 ms detection time over the 200 photolysis events is shown in the inset. (b) Allan deviation of HO_2 concentration. White noise limited trend is also plotted for comparison.

10 ms detection time over the 200 events labeled in Fig. 6(a) is showed in the inset. The Allan deviation plot averaged over all the detection times is shown in Fig. 6(b) and agrees generally with the trend under white noise limited system performance. The Allan deviation of HO_2 concentration for a single photolysis event acquired with 100 µs time resolution is 0.7 ppm, which is equivalent to 7 ppb/$\sqrt{\text{Hz}}$ in terms of bandwidth normalized sensitivity per photolysis event. Since the HO_2 concentration profile is highly reproducible, the line-locked FRS sensitivity is reduced to below 100 ppb with the same time resolution of 100 µs by averaging over 100 such events.

8. Conclusion

We demonstrate HO_2 detection in a photolysis reactor using Faraday rotation spectroscopy. After averaging over 100 photolysis events the current setup allows <100 ppb sensitivity to HO_2 with white noise limited system performance. Implementation of a post-processing digitally balanced detection scheme successfully suppresses absorption from non-paramagnetic species and optical power fluctuations due to parasitic optical fringes. Comparison with conventional laser absorption spectroscopy demonstrates validity of FRS retrievals and supports the claim that FRS enables HO_2 detection when LAS is not applicable due to unknown spectral interference.

With effective suppression of spectral interference and fringe noise, FRS is uniquely suited to perform line-locked measurements, which was demonstrated in this work and opens up the potential of increased time resolution for radical detection in combustion or plasma reactors. This technique also allows measurements at higher pressures including in open environments where line-broadening leads to increased spectral interference and prevents accurate quantification of chemical species with LAS. Thorough system evaluation suggests that the present system is a versatile instrument for sensitive radical quantification in various combustion environments.

Funding. National Science Foundation National Science Foundation Non-Academic Research Internships for Graduate Students (INTERN); National Science Foundation (1507358, 1903362).

Acknowledgments. The authors thank Jonas Westberg for assistance with multi-pass cell modeling and discussions on Faraday rotation spectroscopy.

Disclosures. The authors declare no conflicts of interest.

See Supplement 1 for supporting content.

References

1. J. Zádor, C. A. Taatjes, and R. X. Fernandes, "Kinetics of elementary reactions in low-temperature autoignition chemistry," Prog. Energy Combust. Sci. **37**(4), 371–421 (2011).

Optics EXPRESS

2. F. Battin-Leclerc, "Detailed chemical kinetic models for the low-temperature combustion of hydrocarbons with application to gasoline and diesel fuel surrogates," Prog. Energy Combust. Sci. **34**(4), 440–498 (2008).
3. Y. Ju and W. Sun, "Plasma assisted combustion: Dynamics and chemistry," Prog. Energy Combust. Sci. **48**, 21–83 (2015).
4. S. H. Won, B. Jiang, P. Diévart, C. H. Sohn, and Y. Ju, "Self-sustaining n-heptane cool diffusion flames activated by ozone," Proc. Combust. Inst. **35**(1), 881–888 (2015).
5. Y. Ju, J. K. Lefkowitz, C. B. Reuter, S. H. Won, X. Yang, S. Yang, W. Sun, Z. Jiang, and Q. Chen, "Plasma Assisted Low Temperature Combustion," Plasma Chem. Plasma Process. **36**(1), 85–105 (2016).
6. A. Starikovskiy and N. Aleksandrov, "Plasma-assisted ignition and combustion," Prog. Energy Combust. Sci. **39**(1), 61–110 (2013).
7. C. Yan, C. C. Teng, T. Chen, H. Zhong, A. Rousso, H. Zhao, G. Ma, G. Wysocki, and Y. Ju, "The kinetic study of excited singlet oxygen atom O(1D) reactions with acetylene," Combust. Flame **212**, 135–141 (2020).
8. C. C. Teng, C. Yan, A. Rousso, T. Chen, Y. Ju, and G. Wysocki, "Kinetic Studies of HO2 Radical in a Photolysis Reactor Using Faraday Rotation Spectroscopy," in *Laser Applications to Chemical, Security and Environmental Analysis* (2018).
9. H. Zhong, C. Yan, C. C. Teng, T. Chen, A. Rousso, G. Wysocki, and Y. Ju, "Kinetic studies of excited singlet oxygen atoms O(1D) reactions with fuels in plasma assisted combustion," in *AIAA Scitech 2019 Forum* (2019).
10. W. Sun, S. H. Won, and Y. Ju, "In situ plasma activated low temperature chemistry and the S-curve transition in DME/oxygen/helium mixture," Combust. Flame **161**(8), 2054–2063 (2014).
11. Y. Ju, C. B. Reuter, O. R. Yehia, T. I. Farouk, and S. H. Won, "Dynamics of cool flames," Prog. Energy Combust. Sci. **75**, 100787 (2019).
12. B. Commoner, J. Townsend, and G. E. Pake, "Free Radicals in Biological Materials," Nature **174**(4432), 689–691 (1954).
13. R. Lewicki, J. H. Doty, R. F. Curl, F. K. Tittel, and G. Wysocki, "Ultrasensitive detection of nitric oxide at 5.33 microm by using external cavity quantum cascade laser-based Faraday rotation spectroscopy," Proc. Natl. Acad. Sci. U. S. A. **106**(31), 12587–12592 (2009).
14. B. Brumfield and G. Wysocki, "Faraday rotation spectroscopy based on permanent magnets for sensitive detection of oxygen at atmospheric conditions," Opt. Express **20**(28), 29727 (2012).
15. E. J. Zhang, B. Brumfield, and G. Wysocki, "Hybrid Faraday rotation spectrometer for sub-ppm detection of atmospheric O2," Opt. Express **22**(13), 15957 (2014).
16. Y. Wang, M. Nikodem, E. Zhang, F. Cikach, J. Barnes, S. Comhair, R. A. Dweik, C. Kao, and G. Wysocki, "Shot-noise limited Faraday rotation spectroscopy for detection of nitric oxide isotopes in breath, urine and blood," Sci. Rep. **5**(1), 9096 (2015).
17. N. Wei, B. Fang, W. Zhao, C. Wang, N. Yang, W. Zhang, W. Chen, and C. Fittschen, "Time-Resolved Laser-Flash Photolysis Faraday Rotation Spectrometer: A New Tool for Total OH Reactivity Measurement and Free Radical Kinetics Research," Anal. Chem. **92**(6), 4334–4339 (2020).
18. W. Zhao, G. Wysocki, W. Chen, E. Fertein, D. Le Coq, D. Petitprez, and W. Zhang, "Sensitive and selective detection of OH radicals using Faraday rotation spectroscopy at 28 μm," Opt. Express **19**(3), 2493 (2011).
19. W. Zhao, B. Fang, X. Lin, Y. Gai, W. Zhang, W. Chen, Z. Chen, H. Zhang, and W. Chen, "Superconducting-magnet-based Faraday rotation spectrometer for real time in situ measurement of OH radicals at 10ˆ6 molecule/cmˆ3 level in an atmospheric simulation chamber," Anal. Chem. **90**(6), 3958–3964 (2018).
20. B. Brumfield, W. Sun, Y. Ju, and G. Wysocki, "Direct in situ quantification of HO2 from a flow reactor," J. Phys. Chem. Lett. **4**(6), 872–876 (2013).
21. B. Brumfield, W. Sun, Y. Wang, Y. Ju, and G. Wysocki, "Dual modulation Faraday rotation spectroscopy of HO2 in a flow reactor," Opt. Lett. **39**(7), 1783 (2014).
22. N. Kurimoto, B. Brumfield, X. Yang, T. Wada, P. Dievart, G. Wysocki, and Y. Ju, "Quantitative measurements of HO2/H2O2 and intermediate species in low and intermediate temperature oxidation of dimethyl ether," Proc. Combust. Inst. **35**(1), 457–464 (2015).
23. A. C. Johansson, J. Westberg, G. Wysocki, and A. Foltynowicz, "Optical frequency comb Faraday rotation spectroscopy," Appl. Phys. B **124**(5), 79 (2018).
24. W. Ren, D. F. Davidson, and R. K. Hanson, "IR laser absorption diagnostic for C2H4 in shock tube kinetics studies," Int. J. Chem. Kinet. **44**(6), 423–432 (2012).
25. Z. Hong, R. D. Cook, D. F. Davidson, and R. K. Hanson, "A shock tube study of OH + H2O2 → H2O + HO2 and H2O2 + M → 2OH + M using laser absorption of H2O and OH," J. Phys. Chem. A **114**(18), 5718–5727 (2010).
26. R. K. Hanson and D. F. Davidson, "Recent advances in laser absorption and shock tube methods for studies of combustion chemistry," Prog. Energy Combust. Sci. **44**, 103–114 (2014).
27. D. F. Davidson, A. Y. Chang, and R. K. Hanson, "Laser photolysis shock tube for combustion kinetics studies," Symp. (Int.) Combust., [Proc.] **22**(1), 1877–1885 (1989).